

View of thermodynamic phase transition of the charged Gauss-Bonnet AdS black hole via the shadow

Ke-Jian He(何柯腱), Sen Guo(郭森), Zhi Luo(罗智), and Guo-Ping Li(李国平)

Citation: Chin. Phys. B, 2024, 33 (**4**): 040403. DOI: 10.1088/1674-1056/ad225d
Journal homepage: http://cpb.iphy.ac.cn; http://iopscience.iop.org/cpb

What follows is a list of articles you may be interested in

Thermodynamics in a quantum corrected Reissner-Nordström-AdS black hole and its GUP-corrections

Jian-Jun Song(宋建君) and Cheng-Zhou Liu(刘成周)
Chin. Phys. B, 2024, 33 (**4**): 040402. DOI: 10.1088/1674-1056/ad1a8a

Shadow thermodynamics of AdS black hole with the nonlinear electrodynamics term

He-Bin Zheng(郑何斌), Ping-Hui Mou(牟平辉), Yun-Xian Chen(陈芸仙), and Guo-Ping Li(李国平)
Chin. Phys. B, 2023, 32 (**8**): 080401. DOI: 10.1088/1674-1056/acc806

Thermodynamic effects of Bardeen black hole surrounded by perfect fluid dark matter under general uncertainty principle

Zhenxiong Nie(聂振雄), Yun Liu(刘芸), Juhua Chen(陈菊华), and Yongjiu Wang(王永久)
Chin. Phys. B, 2022, 31 (**5**): 050401. DOI: 10.1088/1674-1056/ac3ca8

Thermodynamics and weak cosmic censorship conjecture of charged AdS black hole in the Rastall gravity with pressure

Xin-Yun Hu(胡馨匀), Ke-Jian He(何柯健), Zhong-Hua Li(李中华), Guo-Ping Li(李国平)
Chin. Phys. B, 2020, 29 (**5**): 050401. DOI: 10.1088/1674-1056/ab7daa

Thermal properties of regular black hole with electric charge in Einstein gravity coupled to nonlinear electrodynamics

Yi-Huan Wei(魏益焕)
Chin. Phys. B, 2019, 28 (**12**): 120401. DOI: 10.1088/1674-1056/ab4e80

View of thermodynamic phase transition of the charged Gauss–Bonnet AdS black hole via the shadow

Ke-Jian He(何柯腱)[1], Sen Guo(郭森)[2], Zhi Luo(罗智)[1], and Guo-Ping Li(李国平)[3,†]

[1] *College of Physics, Chongqing University, Chongqing* 401331, *China*
[2] *Guangxi Key Laboratory for Relativistic Astrophysics, School of Physical Science and Technology, Guangxi University, Nanning* 530004, *China*
[3] *School of Physics and Astronomy, China West Normal University, Nanchong* 637000, *China*

(Received 30 November 2023; revised manuscript received 29 December 2023; accepted manuscript online 25 January 2024)

We examine thermodynamic phase transition (PT) of the charged Gauss–Bonnet AdS black hole (BH) by utilizing the shadow radius. In this system, we rescale the corresponding Gauss–Bonnet coefficient α by a factor of $1/(D-4)$, and ensure that α is positive to avoid any singularity problems. The equation derived for the shadow radius indicates that it increases as the event horizon radius increases, making it an independent variable for determining BH temperature. By investigating the PT curve in relation to shadows, we can observe that the shadow radius can be used as an alternative to the event horizon radius in explaining the phenomenon of BH PT. Furthermore, the results indicate that an increase in the parameter α corresponds to a decrease in the temperature of the BH. By utilizing the relationship between the temperature and the shadow radius, it is possible to obtain the thermal profile of the Gauss–Bonnet AdS BH. It is evident that there is an N-type variation in temperature for pressures $P < P_c$. Additionally, as the parameter α increases, the region covered by shadow expands while the temperature decreases. The utilization of BH shadows as a probe holds immense significance in gaining a deeper understanding of BH thermodynamic behavior.

Keywords: Gauss–Bonnet AdS black hole, thermodynamic, shadow

PACS: 04.70.–s, 04.70.Dy, 04.50.Kd **DOI:** 10.1088/1674-1056/ad225d

1. Introduction

In 2015, the Laser Interferometer Gravitational Wave Observatory (LIGO) made its inaugural announcement of successfully detecting a gravitational wave event generated by the merger of black holes (BHs) in a binary system.[1–3] This discovery provided indirect evidence for the existence of black holes and sparked a renewed interest in searching for these incredibly dense objects in the universe. In 2019, the international collaboration known as the Event Horizon Telescope (EHT) achieved a significant breakthrough in exploring supermassive BHs by capturing an image of one located at the core of M87, a giant elliptical galaxy.[4–9] Recently, the EHT collaboration has captured another image of Sagittarius A* (Sgr A*), which is the supermassive BH located at the center of our galaxy.[10–15] The two ultra-high angular resolution images, resulting from direct human observation of BHs, have successfully confirmed the predictions of general relativity (GR).

The image of Sgr A* exhibits a comparable ring-like structure and shaded areas as those observed in the BH M87*. Due to the strong gravitational effect of BHs, certain photons in the vicinity of the BH are attracted into the BH and cannot reach the position of the distant observer, which forms the shadow of the BH.[16] The ring-like structure surrounding the shadow is called photon ring, which is composed of photons captured due to gravitational bending. By utilizing the BH shadow, one can obtain a deeper understanding of the characteristics of different gravitational spacetimes.

Based on the spacetime background of Schwarzschild BH, Synge pointed out theoretical conditions that photons can escape from the bondage of the BH,[17] and Luminet further studied the image of BH with a thin accretion disk.[18] Different from the shadow of such a non-rotating BH, the shadow of rotating BHs is no longer a standard circle, but a D-shaped shape, which is related to spin parameters.[19,20] At present, the research on BH shadow is more and more in-depth under GR and the modified gravitational background, such as the shape of the non-rotating or rotating BH shadow, considering the observed appearance of the BH shadow with different accretion models, using BH shadows to provide a reference space for the physical parameters in the other modified gravity theories, and looking for the extra dimensions based on BH shadows.[21–40]

On the other hand, drawing upon the groundbreaking research of Hawking and Bekenstein, BHs can be perceived as thermodynamic systems that exhibit numerous parallels with general thermodynamic systems.[41–44] In particular, the phase transition (PT) between the Schwarzschild–AdS BH and the thermal AdS space is studied, which opens the door to the explore of the PT of AdS BHs.[45] The cosmological constant in the thermal system of AdS BHs can be interpreted as a pressure, leading to the observation of thermodynamic PT. The thermodynamic PT process has been extensively investigated in other modified gravitational theories, leading to the discov-

†Corresponding author. E-mail: gpliphys@yeah.net

© 2024 Chinese Physical Society and IOP Publishing Ltd

ery of intriguing findings.[46–57] Among them, Kubiznak *et al.* studied the *P*–*V* criticality and the van der Waals (vdW)-like PT of the charged AdS BH, it shows that the BH system bears a resemblance to the liquid–gas system.[46] The thermodynamic PTs have expanded to include additional types, such as the triple point PT and the reentrant PT.[47–49]

In the framework of AdS BHs as strong gravitational systems, it is interesting to study the relationship with its dynamics and thermodynamics. The BH shadow provides us with an opportunity to study thermodynamic PTs for AdS BHs. In Refs. [58–60], Wei *et al.* investigated the connection between thermodynamic PTs and photon orbits for AdS BHs using null geodesics. Recently, Zhang *et al.* found that the phase structure can be investigated via the shadow radius for the spherically symmetric BH model.[61] In addition, Belhaj *et al.* built a thermal profile between the BH temperature and shadow under the AdS charged spacetime.[62] In the context of the Reissner–Nordström–AdS BH and the Kerr AdS BH, one can find that the shadow radius can reflect the microstructure of the BH.[63] Moreover, Wang *et al.* studied the relation between the Ruppeiner geometry and the shadow radius for the Reissner–Nordström–AdS BH, and the result shows that the phase structure and the microstructure of BHs can be investigated using the shadow radius.[64] For regular AdS BHs, by establishing the connections between thermodynamic PTs and BH shadow, the results showed that there exist N-type changes in thermal profiles.[65]

Inspired by these pioneering works, we study the thermodynamic PT by the shadow of a charged Gauss–Bonnet AdS BH.[66,67] The Gauss–Bonnet gravity is one of the higher order derivative curvature gravities, and the four-dimensional Gauss–Bonnet gravity is recently investigated by Glavan and Lin.[66] The Gauss–Bonnet (GB) coefficient α is rescaled by a factor $1/(D-4)$, and then the GB term generates nontrivial dynamics. In addition, in the context of the positive GB term, there exists a static spherically symmetric BH without the singularity. In the four-dimensional Gauss–Bonnet spacetime, the motion of a spinning test particle is studied.[68] In Ref. [69], the causality of four-dimensional Gauss–Bonnet BHs was investigated. Moreover, Guo *et al.* studied the innermost stable circular orbit and shadow of the Gauss–Bonnet BH,[70] and the shadow of the rotating BH was also studied in Ref. [71]. In the extended phase space, the thermodynamic properties of the Gauss–Bonnet BH were widely studied.[72–79] At present, there are few studies discussing the thermodynamic properties based on the shadow of the Gauss–Bonnet BH, which presents an intriguing research opportunity. Considering that current observational methods make it difficult to directly detect the thermodynamic PT of a BH, this paper establishes the relationship between the BH shadow and its thermodynamic PT. We investigate the influence of the GB coefficient α on thermodynamic PTs in a charged Gauss–Bonnet AdS BH. The findings indicate that the BH shadow has potential to enhance our comprehension of BH thermodynamics, potentially introducing a new observational approach for investigating strong gravity systems.

The rest of this paper is organized as follows. In Section 2, the derivation of the shadow radius expression is briefly reviewed. In Section 3, the thermodynamic PT is investigated by the shadow radius for the charged Gauss–Bonnet AdS BH. In Section 4, the thermal profiles of the charged Gauss–Bonnet AdS BH are studied. The conclusions are given in Section 5. In this study, we use the units $G = c = \hbar = \kappa = 1$.

2. Shadows of the charged Gauss–Bonnet AdS black hole

We start with the shadow of a charged Gauss–Bonnet AdS BH. By considering the spherically symmetric spacetime, the line element of charged Gauss–Bonnet AdS BH has the form[66,67]

$$\mathrm{d}s^2 = -f(r)\mathrm{d}t^2 + \frac{\mathrm{d}r^2}{g(r)} + r^2(\mathrm{d}\theta^2 + \sin^2\theta\mathrm{d}\phi^2), \tag{1}$$

where $f(r)$ and $g(r)$ are the functions of the radius r. In this spacetime, the behavior of the test particle, i.e., the photon in the vicinity of the BH can be described by the Euler–Lagrangian equation, which is

$$\frac{\mathrm{d}}{\mathrm{d}\tau}\frac{\partial\mathcal{L}}{\partial\dot{x}^\mu} - \frac{\partial\mathcal{L}}{\partial x^\mu} = 0. \tag{2}$$

Here, τ is affine parameter, while $\dot{x}^\mu$ denotes the four-velocity of photon. The Lagrangian density $\mathcal{L}$ is

$$2\mathcal{L} = g^{\mu\nu}\frac{\mathrm{d}x^\mu}{\mathrm{d}\tau}\frac{\mathrm{d}x^\nu}{\mathrm{d}\tau} = -m^2, \tag{3}$$

with $m^2 = 0$ for the photon. In the background of the static spherically symmetric spacetime, the trajectory of a photon is confined to the equatorial plane of the BH, namely $\theta = \pi/2$ and $\dot{\theta} = 0$. Consequently, it is possible to deduce

$$-\frac{p_t^2}{2f(r)} + \frac{g(r)p_r^2}{2} + \frac{p_\phi^2}{2r^2} = 0. \tag{4}$$

Since the metric is independent of both the time t and the azimuthal angle ϕ, two quantities are conserved, namely the energy E and the orbital angular momentum L of the photon as follows:

$$E = -g_{tt}\frac{\mathrm{d}t}{\mathrm{d}\tau} = f(r)\frac{\mathrm{d}t}{\mathrm{d}\tau},\ \ L = -g_{\phi\phi}\frac{\mathrm{d}\phi}{\mathrm{d}\tau} = r^2\frac{\mathrm{d}\phi}{\mathrm{d}\tau}. \tag{5}$$

By utilizing the null geodesic condition $g_{\mu\nu}\dot{x}^\mu\dot{x}^\nu = 0$, one can obtain the equation of motion of the photon as follows:

$$\begin{aligned}&\frac{\mathrm{d}t}{\mathrm{d}\tau} = \frac{E}{f(r)},\ \ \frac{\mathrm{d}\phi}{\mathrm{d}\tau} = \frac{L}{r^2},\\ &\frac{\mathrm{d}r}{\mathrm{d}\tau} = \pm\frac{\sqrt{g(r)r^2(E^2r^2 - L^2f(r))}}{r^2\sqrt{f(r)}}.\end{aligned} \tag{6}$$

The symbol $\pm$ in the above equation denotes the counterclockwise ($-$) and clockwise ($+$) directions of photon motion. With the help of Eq. (3), the equation of the geodesic motion for the photon can be written as

$$\dot{r}^2 + V_{\rm eff}(r) = 0, \tag{7}$$

where the term of $V_{\rm eff}(r)$ is called effective potential

$$V_{\rm eff}(r) = g(r)\Big(\frac{L^2}{r^2} - \frac{E^2}{f(r)}\Big). \tag{8}$$

The effective potential at the location of the photon ring ($r_{\rm ph}$) satisfies the following condition:

$$V_{\rm eff}(r_{\rm ph}) = 0, \;\; V'_{\rm eff}(r_{\rm ph}) = 0, \;\; V''_{\rm eff}(r_{\rm ph}) > 0, \tag{9}$$

in which the prime presents the derivation with respect to r. According to Eqs. (8) and (9), one can obtain the impact parameter, that is,

$$\frac{L}{E} = \frac{r_{\rm ph}}{\sqrt{f(r_{\rm ph})}}\Big|_{r_{\rm ph}}. \tag{10}$$

Meanwhile, we can get the parameterized orbit of the photon as follows:

$$\frac{{\rm d}r}{{\rm d}\phi} = \frac{\dot{r}}{\dot{\phi}} = \frac{r^2 g(r) p_r}{L}. \tag{11}$$

Employing Eqs. (4) and (11) one can obtain

$$\frac{{\rm d}r}{{\rm d}\phi} = \pm r\sqrt{g(r)\Big(\frac{r^2E^2}{L^2 f(r)} - 1\Big)}. \tag{12}$$

By choosing $\frac{{\rm d}r}{{\rm d}\phi}\big|_{r=\chi} = 0$, the position where the photon orbit is deflected near the BH is

$$\frac{{\rm d}r}{{\rm d}\phi} = \pm r\sqrt{g(r)\Big(\frac{r^2 f(\chi)}{\chi^2 f(r)} - 1\Big)}. \tag{13}$$

When the light emitted from a static observer, with an emission angle of β relative to the radial direction, one can obtain[61–64]

$$\cot\beta = \frac{\sqrt{g_{rr}}}{\sqrt{g_{\phi\phi}}}\frac{{\rm d}r}{{\rm d}\phi}\Big|_{r=r_{\rm obs}} = \pm\sqrt{\frac{r^2_{\rm obs} f(\chi)}{\chi^2 f(r_{\rm obs})} - 1}, \tag{14}$$

where the position of observer is $r = r_{\rm obs}$. By combining Eqs. (13) and (14), the radius of BH shadow observed by the observer is

$$r_{\rm s} = r_{\rm obs}\sin\beta = \chi\sqrt{\frac{f(r_{\rm obs})}{f(\chi)}}\Big|_{\chi\to r_{\rm ph}}. \tag{15}$$

The metric of a charged Gauss–Bonnet AdS BH is given by[66,67]

$$f(r) = g(r)^{-1} = 1 + \frac{r^2}{2\alpha}\Big[1 - \sqrt{1 + 4\alpha\Big(\frac{2M}{r^3} - \frac{Q^2}{r^4} - \frac{8\pi P}{3}\Big)}\Big], \tag{16}$$

where M denotes the BH mass, Q represents the BH charge, and α represents the GB coefficient with dimension. It is worth noting that the cosmological constant term $1/l^2$ is replaced by the term $8\pi P/3$ in Eq. (16), and P is the pressure of the BH. Hence, the photon circular orbit radius can be determined with the aid of Eqs. (9) and (16), which is

$$\begin{aligned} &-2\alpha(3Q^2 - 6Mr_{\rm ph} + 8P\pi r^4_{\rm ph}) \\ &+3r^2_{\rm ph}(2Q^2 + r_{\rm ph}(-3M + r_{\rm ph})) = 0. \end{aligned} \tag{17}$$

Moreover, the expression of the shadow radius for a charged Gauss–Bonnet AdS BH is also obtained by using Eqs. (16) and (15), that is,

$$r_{\rm s} = r_{\rm ph}\sqrt{\frac{f(r_{\rm obs})}{f(r_{\rm ph})}}. \tag{18}$$

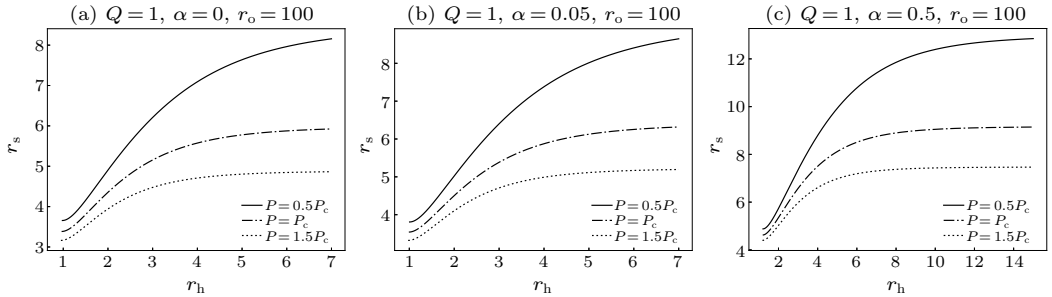


Fig. 1. The relation between the shadow radius $r_{\rm s}$ and the event horizon radius $r_{\rm h}$ for the charged Gauss–Bonnet AdS BH. (a) GB coefficient $\alpha = 0$ (RN-AdS BH), (b) GB coefficient $\alpha = 0.05$, (c) GB coefficient $\alpha = 0.5$. Here, $P = 0.5P_{\rm c}$, $P = P_{\rm c}$, and $P = 1.5P_{\rm c}$ are represented by the solid, segment point, and dotted lines, respectively.

For a distant static observer, it follows that the limiting condition at infinity is $f(r) \to 1$.[61] In Fig. 1, we give the correlation between the shadow radius $r_{\rm s}$ and the event horizon radius $r_{\rm h}$ in Fig. 1, where the position of the observer is fixed as $r_{\rm obs} = 100$. From the left to right panel of Fig. 1, the value of the GB coefficient α is taken as $\alpha = 0$, $\alpha = 0.05$, and $\alpha = 0.5$. The variation in the GB coefficient α will have an impact on the event horizon radius of the BH, with a corresponding effect on the radius of its shadow. As shown in Fig. 1, as the GB coefficient α increases, the BH shadow radius $r_{\rm s}$ corresponding to the event horizon radius $r_{\rm h}$ becomes larger. A higher value of α leads to a greater increase in shadow radius $r_{\rm s}$ with

increasing event radius $r_{\rm h}$, resulting in an increased slope of the relationship curve between $r_{\rm s}$ and $r_{\rm h}$. Although the value of the GB coefficient α varies, the shadow radius $r_{\rm s}$ always behaves as a monotonically increasing function of the event radius $r_{\rm h}$, and the relation between them is positively correlated. In other words, the temperature of a BH can be described by the shadow radius $r_{\rm s}$ instead of the event horizon radius $r_{\rm h}$.

3. Phase transitions of the charged Gauss–Bonnet AdS black hole through shadow analysis

For a charged Gauss–Bonnet AdS BH, with the constraint $f(r)=0$, it is allowed us to obtain the expressions of mass M and temperature T of the BH,

$$M=\frac{Q^2}{2r_{\rm h}}+\frac{\alpha}{2r_{\rm h}}+\frac{r_{\rm h}}{2}+\frac{4\pi P}{3}r_{\rm h}^3,$$
$$T=\frac{2r_{\rm h}^3}{r_{\rm h}^2+\alpha}P-\frac{Q^2-r_{\rm h}^2+\alpha}{4\pi r_{\rm h}(r_{\rm h}^2+2\alpha)}. \tag{19}$$

Furthermore, the equation of state is

$$P=\left(\frac{\alpha}{r_{\rm h}^3}+\frac{1}{2r_{\rm h}}\right)T+\frac{Q^2+\alpha-r_{\rm h}^2}{8\pi r_{\rm h}^4}. \tag{20}$$

Utilizing Eq. (20) and the critical condition $(\partial P/\partial r_{\rm h})=0=(\partial^2 P/\partial r_{\rm h}^2)$, one can obtain the critical point for the spacetime (16) as follows:

$$P_{\rm c}=\frac{30\alpha^2+36\alpha Q^2+9Q^4-(4\sqrt{3}\alpha-3\sqrt{3}Q^2)\sqrt{16\alpha^2+16\alpha Q^2+3Q^4}}{576\pi(\alpha^3+\alpha^2Q^2)}\simeq-\frac{25\alpha}{864\pi Q^4}+\frac{1}{96\pi Q^2}, \tag{21}$$

$$r_{\rm c}=\sqrt{6\alpha+3Q^2+\sqrt{3}\sqrt{16\alpha^2+16\alpha Q^2+3Q^4}}\simeq\frac{7\alpha}{\sqrt{6}Q}+\sqrt{6}Q, \tag{22}$$

$$T_{\rm c}=\frac{\sqrt{6\alpha+3Q^2+\sqrt{48\alpha^2+48\alpha Q^2+9Q^4}}}{3\pi(8\alpha+3Q^2+\sqrt{48\alpha^2+48\alpha Q^2+9Q^4})}\simeq\frac{1}{3\sqrt{6}\pi Q}-\frac{\alpha}{2\sqrt{6}\pi(Q^2)^{3/2}}. \tag{23}$$

Based on Eqs. (19) and (18), the temperature trend with event radius $r_{\rm h}$ and shadow radius $r_{\rm s}$ is shown, see Fig. 2. In the case of GB coefficient $\alpha=0.01$, the temperature of BH as a function of $r_{\rm h}$ under the different pressure $P=0.5P_{\rm c}$, $P=P_{\rm c}$, and $P=1.5P_{\rm c}$ are shown in Fig. 2(a). The results indicate the presence of a van der Waals-like PT at a pressure of $0.5P_{\rm c}$, where the region with a small radius corresponds to the fluid phase, while the region with a large radius corresponds to the gas phase. At a pressure of $P=P_{\rm c}$, an unstable BH phase emerges. Furthermore, there is no observed PT at a pressure of $1.5P_{\rm c}$.

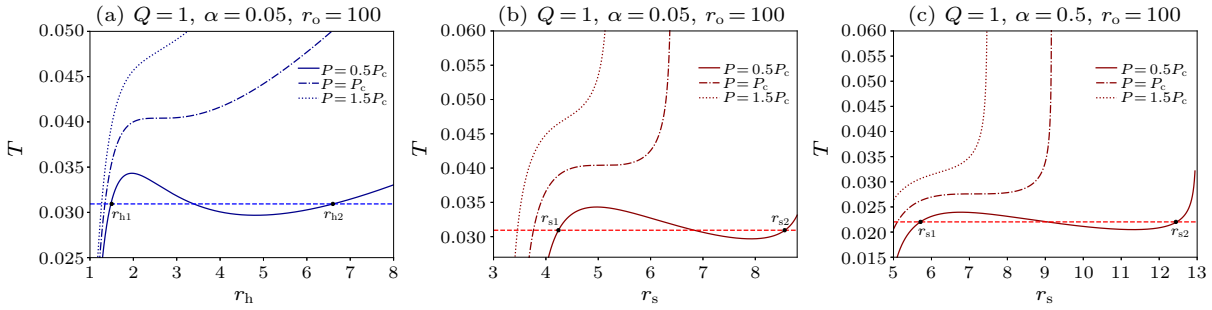


Fig. 2. The temperature of the charged Gauss–Bonnet AdS BH in relation to its event horizon $r_{\rm h}$ and shadow $r_{\rm s}$. (a) Temperature as a function of $r_{\rm h}$ with GB coefficient $\alpha=0.05$, (b) temperature as a function of $r_{\rm s}$ with GB coefficient $\alpha=0.05$, (c) temperature as a function of $r_{\rm s}$ with GB coefficient $\alpha=0.5$. Here, $P=0.5P_{\rm c}$, $P=P_{\rm c}$, and $P=1.5P_{\rm c}$ are represented by the solid, segment point, and dotted lines, respectively.

The relation between the thermodynamics and shadow radius $r_{\rm s}$ under the different pressures are shown in Figs. 2(b) and 2(c), where the values of α are, in turn, $\alpha=0.05$ and $\alpha=0.5$. Although the temperature change of a BH is described in terms of the shadow radius instead of the event horizon radius, it still effectively shows the PT process of the BH. From Figs. 2(b) and 2(c), it shows that there exist a stable small BH when $r_{\rm s}<r_{\rm s1}$ and a stable large BH when $r_{\rm s}>r_{\rm s2}$. When $r_{\rm s1}<r_{\rm s}<r_{\rm s2}$, there exists an unstable intermediate BH. For three cases of the pressure, one can find that the PT process in the context of the shadow radius is similar to the left panels of Fig. 2. In addition, with the increase of the GB coefficient α, the PT temperature decreases and the shadow radius increases. Indeed, the determination of the PT grade can be achieved through the analysis of heat capacity. Under the constant pressure, the heat capacity of the charged Gauss–Bonnet

AdS BH can be expressed as

$$C_{\rm P} = T\left(\frac{{\rm d}S}{{\rm d}T}\right)_{P,Q,\alpha} = \frac{8\pi r_{\rm h}^2(2\alpha + r_{\rm h}^2)(-\alpha - Q^2 + r_{\rm h}^2 + 8P\pi r_{\rm h}^4)}{2\alpha^2 + 3Q^2 r_{\rm h}^2 - r_{\rm h}^4 + 8P\pi r_{\rm h}^6 + \alpha(2Q^2 + 5r_{\rm h}^2 + 48P\pi r_{\rm h}^4)}. \tag{24}$$

As shown in Fig. 3, we plot the the relationship of heat capacity with the radius of the event horizon ($C_{\rm P}$–$r_{\rm h}$) and with the radius of the shadow ($C_{\rm P}$–$r_{\rm s}$). In Fig. 3(a), it shows that there exists a specific heat diverge at the critical point, which represents a second-order PT. Results for the shadow radius $r_{\rm s}$ decreasing are similar to those for the event horizon radius $r_{\rm h}$ in Figs. 3(b) and 3(c).

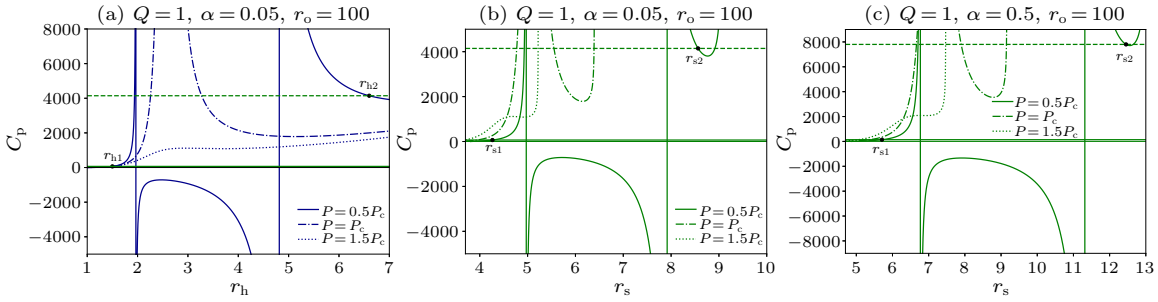


Fig. 3. The heat capacity $C_{\rm P}$ as a function of the event horizon radius and the shadow radius for the charged Gauss–Bonnet AdS BH: (a) heat capacity changing with $r_{\rm h}$ for $\alpha = 0.05$, (b) heat capacity changing with $r_{\rm s}$ for $\alpha = 0.05$, (c) heat capacity changing with $r_{\rm s}$ for $\alpha = 0.5$. Here, $P = 0.5P_{\rm c}$, $P = P_{\rm c}$, and $P = 1.5P_{\rm c}$ are represented by the solid, segment point, and dotted lines, respectively.

4. Thermal profile of the charged Gauss–Bonnet AdS black hole

For a distant observer ($r_{\rm o} \to \infty$), the apparent shape of the BH shadow can be determined by constructing celestial coordinates (x, y),[80]

$$x = \lim_{r_{\rm o}\to\infty}\left(-r^2 \sin\theta_{\rm o}\frac{{\rm d}\phi}{{\rm d}r}\right)|_{\theta_{\rm o}\to\frac{\pi}{2}},$$
$$y = \lim_{r_{\rm o}\to\infty}\left(r^2\frac{{\rm d}\theta}{{\rm d}r}\right)|_{\theta_{\rm o}\to\frac{\pi}{2}}. \tag{25}$$

Here, the celestial coordinate x denotes the apparent perpendicular distance of the image observed from the axis of symmetry, and the celestial coordinate y denotes the apparent perpendicular distance projected on the equatorial plane. In addition, the term $r_{\rm o}$ represents the observer's distance from the BH, while $\theta_{\rm o}$ denotes the inclination angle between the observer's line of sight and the axis of BH. Therefore, the shadow contour cast by the charged Gauss–Bonnet AdS BH in the observer's sky can be obtained, see Fig. 4. The relationship between the change in pressure and the radius of the BH shadow is demonstrated, indicating that an increase in pressure directly corresponds to an decrease of the shadow radius. However, the larger the value of the GB coefficient α is, the greater the shadow radius will be.

By combining the temperature and shadow of BH, one can build the BH thermal profile in the shadow contour panel. Similarly, we consider the effect of changes in pressure P and system parameter α on the thermal profile of the BH. In Fig. 5, the gradual increase in pressure as $P = 0.5P_{\rm c}$, $P = P_{\rm c}$, $P = 1.5P_{\rm c}$, corresponding to the left, middle, and right columns, respectively. The first row is $\alpha = 0.05$, the second row is $\alpha = 0.5$. The result indicate that as pressure increases, the radius of the thermal profile decreases while the temperature of the BH rises. Figures 5(a) and 5(d) correspond to $P < P_{\rm c}$, indicating there exists an N-type change trend of the BH temperature. Figures 5(c) and 5(e) correspond to the case where $P = P_{\rm c}$, indicating a constant temperature within the critical region and thermodynamic instability of the BH. Figures 5(c) and 5(f) correspond to $P > P_{\rm c}$, wherein the temperature of the BH gradually diminishes from the boundary towards the center of its shadow.

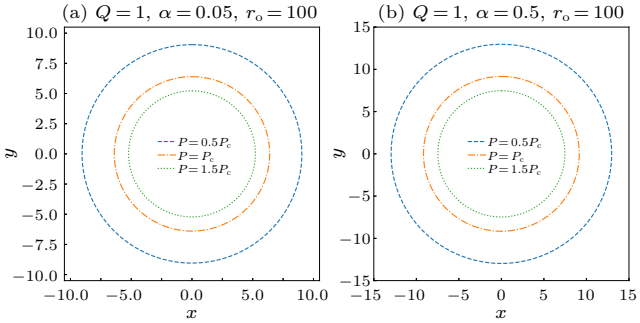


Fig. 4. The shadow cast by the charged Gauss–Bonnet AdS BH varies under different pressures and α: (a) the GB coefficient $\alpha = 0.05$, (b) the GB coefficient $\alpha = 0.5$. In addition, the mass of BH and distance of observer is taken as $M = 60$ and $r_{\rm o} = 100$.

To study the N-type change trend from $r_{\rm s1}$ to $r_{\rm s2}$ for $P < P_{\rm c}$, we plot the thermal profile of BHs in Fig. 6. It is shown that a pattern of temperature fluctuations, initially rising and then falling before ultimately rising again as the shadow radius increases. These observations align with the outcomes depicted in Fig. 2. In addition, the PT temperature decreases with the increasing GB coefficient α and the unstable PT region becomes larger. Hence, the results indicate that the thermal profile can reflect the PT for the charged Gauss–Bonnet AdS BH.

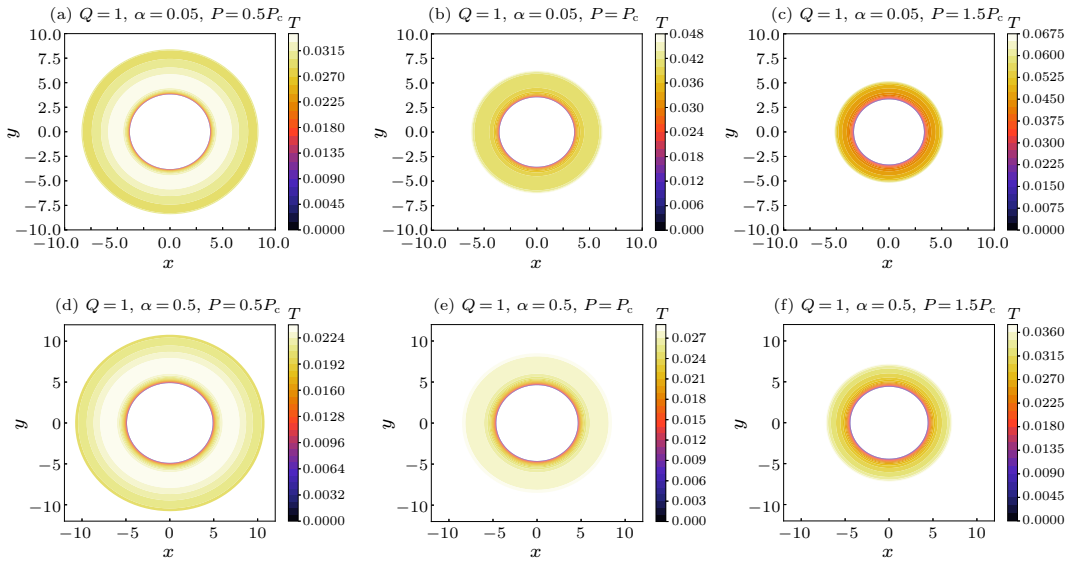


Fig. 5. Thermal profile of the charged Gauss–Bonnet AdS BH. The mass of BH and distance of observer is taken as $M = 60$ and $r_o = 100$.

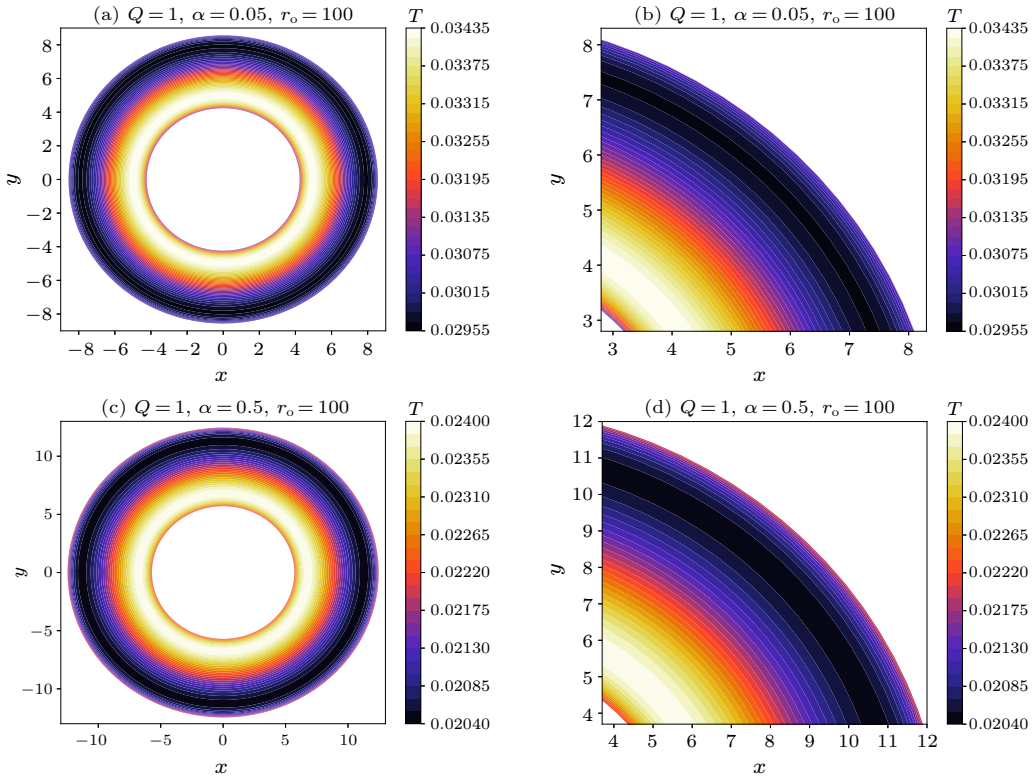


Fig. 6. Thermal profile of the charged Gauss–Bonnet AdS BH in the region of r_{s1} to r_{s2} for $P < P_c$. The mass of BH and distance of observer is taken as $M = 60$ and $r_o = 100$.

5. Discussion and conclusion

In this study, we investigate the relationship between the BH shadow and the thermodynamics for the charged Gauss–Bonnet AdS BH. Initially, we examine the motion of a photon in the equatorial plane of the BH by utilizing the Euler–Lagrangian equation to obtain the radius of the BH shadow. Our findings indicate a positive correlation between the shadow radius r_s and event horizon radius r_h, with an observed increase in shadow radius as event horizon radius increases. This implies that it is possible to express BH temperature in terms of its shadow radius. Furthermore, variations in parameters also impact both event horizon and shadow radius. Specifically, as the GB coefficient α increases, there is a corresponding enlargement in both BH shadow radius r_s and event horizon radius r_h.

In the context of the shadow, the equation of state and the critical point are calculated. The utilization of shadow radius r_s as an alternative parameter reveals that the BH still under-

goes a PT akin to when event horizon radius $r_{\rm h}$ is employed as a parameter. It is shown that in both the T–$r_{\rm h}$ and T–$r_{\rm s}$ curves, for $P > P_{\rm c}$ there exist supercritical phases, for $P = P_{\rm c}$ there exist thermodynamically unstable phases, and for $P < P_{\rm c}$ there exist three branches of BH states, i.e., small BH, intermediate BH, and large BH. The noteworthy point is that when the pressure $P < P_{\rm c}$, for both T–$r_{\rm h}$ and T–$r_{\rm s}$ curves, there exist oscillatory curves of the temperatures, which give the coexistence region of the small/large BH and the presence of the first-order PT. Meanwhile, for the same pressure P, with the increase of GB coefficient α, the PT temperature T decreases and the shadow radius $r_{\rm s}$ increases.

Additionally, the thermal profile of the charged Gauss–Bonnet AdS BH is constructed for various values of the GB coefficient α. We analyze the shape of BH shadow as perceived by an observer located at a considerable distance. The result shows that the increases in pressure and the GB coefficient α lead to an observed increase in the shadow radius. By combining temperature and shadow casting, the thermal profile in the shadow profile panel is constructed. One can find that with the increase of pressure, the thermal profile radius and the BH temperature decrease and increases, respectively. Meanwhile, for the pressure $P = 0.5P_{\rm c}$, $P = P_{\rm c}$, and $P = 1.5P_{\rm c}$, there are three trends in the change of the BH temperature as the thermal profile radius increases. When $P < P_{\rm c}$, there exists the N-type change trend for the BH temperature. When $P = P_{\rm c}$, the BH is thermodynamically unstable, the corresponding temperature remains stable in the critical region. When $P > P_{\rm c}$, as the thermal profile radius increases, the BH temperature decreases. The thermal profile of the region from $r_{\rm s1}$ to $r_{\rm s2}$ is also presented, specifically aiming to further investigate the N-type change trend for $P < P_{\rm c}$. It indicate that with the increase of the shadow radius, there is an initial rise followed by a decline and then another rise in the corresponding temperature. Moreover, for a larger GB coefficient α and a wider unstable PT region, the corresponding temperature tends to decrease.

We end with a brief summary. The shadow of a BH, as a feature with promising observational prospects, is closely linked to the thermodynamic behavior of the BH and holds significant potential in unveiling its thermodynamic properties. However, when we utilize the radius of the BH shadow instead of the event horizon radius to describe BH thermodynamics, it is important to note that the shadow radius, being an observed quantity from an astronomical perspective, may not be exactly identical to the event horizon radius. Whether some of the properties of the event horizon of a BH can also be reflected in the shadow needs more observational data in the future to verify.

Acknowledgments

Project supported by the National Natural Science Foundation of China (Grant No. 11903025), the starting fund of China West Normal University (Grant No. 18Q062), the Sichuan Youth Science and Technology Innovation Research Team (Grant No. 21CXTD0038), the Chongqing Science and Technology Bureau (Grant No. cstc2022ycjh-bgzxm0161), and the Natural Science Foundation of Sichuan Province (Grant No. 2022NSFSC1833).

References

[1] Abbott B P *et al.* 2016 *Phys. Rev. Lett.* **116** 241103
[2] Abbott B P *et al.* 2016 *Phys. Rev. Lett.* **116** 241102
[3] Abbott B P *et al.* 2016 *Phys. Rev. Lett.* **116** 061102
[4] Akiyama K *et al.* 2019 *Astrophys. J. Lett.* **875** L1
[5] Akiyama K *et al.* 2019 *Astrophys. J. Lett.* **875** L2
[6] Akiyama K *et al.* 2019 *Astrophys. J. Lett.* **875** L3
[7] Akiyama K *et al.* 2019 *Astrophys. J. Lett.* **875** L4
[8] Akiyama K *et al.* 2019 *Astrophys. J. Lett.* **875** L5
[9] Akiyama K *et al.* 2019 *Astrophys. J. Lett.* **875** L6
[10] Akiyama K *et al.* 2022 *Astrophys. J. Lett.* **930** L12
[11] Akiyama K *et al.* 2022 *Astrophys. J. Lett.* **930** L13
[12] Akiyama K *et al.* 2022 *Astrophys. J. Lett.* **930** L14
[13] Akiyama K *et al.* 2022 *Astrophys. J. Lett.* **930** L15
[14] Akiyama K *et al.* 2022 *Astrophys. J. Lett.* **930** L16
[15] Akiyama K *et al.* 2022 *Astrophys. J. Lett.* **930** L17
[16] Wald R M 1984 *General Relativity* (The University of Chicago Press)
[17] Synge J L 1966 *Mon. Not. R. Astron. Soc.* **131** 463
[18] Luminet J P 1979 *Astron. Astrophys.* **75** 228
[19] Bardeen J M 1973 *Timelike and null geodesics in the Kerr metric, in black holes*. In: *Proceedings, Ecole d'Eté de Physique Théorique: Les Astres Occlus*, Les Houches, France, August 1972, pp. 215–240
[20] Chandrasekhar S 1983 *The Mathematical Theory of Black Holes* (Oxford: Oxford University Press)
[21] Banerjee I, Chakraborty S and SenGupta S 2020 *Phys. Rev. D* **101** 041301
[22] Safarzadeh M, Loeb A and Reid M 2019 *Mon. Not. R. Astron. Soc.* **488** L90
[23] Amarilla L, Eiroa E F and Giribet G 2010 *Phys. Rev. D* **81** 124045
[24] Grenzebach A, Perlick V and ämmerzahl C L 2014 *Phys. Rev. D* **89** 124004
[25] Hu Z, Zhong Z, Li P C, Guo M and Chen B 2021 *Phys. Rev. D* **103** 044057
[26] Wei S W and Liu Y X 2013 *J. Cosmol. Astropart. Phys.* **11** 063
[27] Wang H M, Xu Y M and Wei S W 2019 *J. Cosmol. Astropart. Phys.* **03** 046
[28] Narayan R, Johnson M D and Gammie C F 2019 *Astrophys. J.* **885** L33
[29] Gralla S E, Holz D E and Wald R M 2019 *Phys. Rev. D* **100** 024018
[30] Zeng X X, Zhang H Q and Zhang H 2020 *Eur. Phys. J. C* **80** 872
[31] Peng J, Guo M and Feng X H 2021 *Chin. Phys. C* **45** 085103
[32] He K J, Tan S C and Li G P 2022 *Eur. Phys. J. C* **82** 81
[33] Li G P and He K J 2021 *Eur. Phys. J. C* **81** 1018
[34] Zeng X X, He K J and Li G P 2022 *Sci. China Phys. Mech. Astron.* **65** 290411
[35] Li G P and He K J 2021 *J. Cosmol. Astropart. Phys.* **06** 037
[36] He K J, Guo S, Tan S C and Li G P 2022 *Chin. Phys. C* **46** 085106
[37] Guo S, Li G R and Liang E W 2022 *Phys. Rev. D* **105** 023024
[38] Zhu Y and Wang T 2021 *Phys. Rev. D* **104** 104052
[39] Gan Q, Wang P, Wu H W and Yang H T 2021 *Phys. Rev. D* **104** 044049
[40] He K J, Zhang X and Li X 2022 *Chin. Phys. C* **46** 075103
[41] Hawking S W 1975 *Commun. Math. Phys.* **43** 199
[42] Hawking S W 1976 *Phys. Rev. D* **13** 191
[43] Bekenstein J D 1972 *Lett. Nuovo Cim.* **4** 737
[44] Bekenstein J D 1974 *Phys. Rev. D* **9** 3292
[45] Hawking S W and Page D N 1983 *Commun. Math. Phys.* **87** 577
[46] Kubiznak D and Mann R B 2012 *J. High Energy Phys.* **2012** 033
[47] Altamirano N, Kubizňák D, Mann R B and Sherkatghanad Z 2014 *Class. Quantum Grav.* **31** 042001

[48] Altamirano N, Kubiznak D and Mann R B 2013 *Phys. Rev. D* **88** 101502
[49] Wei S W and Liu Y X 2014 *Phys. Rev. D* **90** 044057
[50] Hendi S H, Panahiyan S and Eslam Panah B 2015 *Int. J. Mod. Phys. D* **25** 1650010
[51] Kubiznak D and Simovic F 2016 *Class. Quantum Grav.* **33** 245001
[52] Hendi S H, Eslam Panah B and Panahiyan S 2015 *J. High Energy Phys.* **2015** 157
[53] Hendi S H, Panahiyan S, Panah B E and Armanfard Z 2016 *Eur. Phys. J. C* **76** 396
[54] Hennigar R A, Mann R B and Tjoa E 2017 *Phys. Rev. Lett.* **118** 021301
[55] Hendi S H, Eslam Panah B, Panahiyan S and Talezadeh M S 2017 *Eur. Phys. J. C* **77** 133
[56] Jafarzade K, Sadeghi J, Panah B E and Hendi S H 2021 *Annals Phys.* **432** 168577
[57] Kubiznak D, Mann R B and Teo M 2017 *Class. Quantum Grav.* **34** 063001
[58] Wei S W and Liu Y X 2018 *Phys. Rev. D* **97** 104027
[59] Chandrasekhar B and Mohapatra S 2019 *Phys. Lett. B* **791** 367
[60] Zhang M, Han S Z, Jiang J and Liu W B 2019 *Phys. Rev. D* **99** 065016
[61] Zhang M and Guo M 2020 *Eur. Phys. J. C* **80** 790
[62] Belhaj A, Chakhchi L, El Moumni H, Khalloufi J and Masmar K 2020 *Int. J. Mod. Phys. A* **35** 2050170
[63] Cai X C and Miao Y G 2021 arXiv:2107.08352 [gr-qc]
[64] Wang C, Wu B, Xu Z M and Yang W L 2022 *Nucl. Phys. B* **976** 115698
[65] Guo S, Li G R and Li G P 2022 2022 *Chin. Phys. C* **46** 095101
[66] Glavan D and Lin C 2020 *Phys. Rev. Lett.* **124** 081301
[67] Fernandes P G S 2020 *Phys. Lett. B* **805** 135468
[68] Zhang Y P, Wei S W and Liu Y X 2020 *Universe* **6** 103
[69] Ge X H and Sin S J 2020 *Eur. Phys. J. C* **80** 695
[70] Guo M and Li P C 2020 *Eur. Phys. J. C* **80** 588
[71] Wei S W and Liu Y X 2021 *Eur. Phys. J. Plus* **136** 436
[72] Hosseini Mansoori S A 2021 *Phys. Dark Univ.* **31** 100776
[73] Hegde K, Naveena Kumara A, Rizwan C L A, Ali M S and Ajith K M 2021 *Ann. Phys.* **429** 168461
[74] Wang Y Y, Su B Y and Li N 2021 *Phys. Dark Univ.* **31** 100769
[75] Ghosh S G, Singh D V, Kumar R and Maharaj S D 2021 *Ann. Phys.* **424** 168347
[76] Li H L, Zeng X X and Lin R 2020 *Eur. Phys. J. C* **80** 652
[77] Wei S W and Liu Y X 2020 *Phys. Rev. D* **101** 104018
[78] Zeng X. X, Hu X Y and He K J 2019 *Nucl. Phys. B* **949** 114823
[79] Singh D V and Siwach S 2020 *Phys. Lett. B* **808** 135658
[80] Eiroa E F and Sendra C M 2018 *Eur. Phys. J. C* **78** 91